Monitoring the fate of injected carbon dioxide using geodetic techniques

D. W. Vasco[1], T. Dixon[2], A. Ferretti[3], and S. V. Samsonov[4]

1 Energy Geosciences Division, Lawrence Berkeley National Laboratory, University of California, Berkeley, CA, USA

2 University of South Florida, School of Geosciences, 4202 E. Fowler Ave, Tampa, FL, USA

3 TRE ALTAMIRA Srl, Ripa di Porta Ticinese, 79, 20143, Milan, Italy

4 Canada Centre for Mapping and Earth Observation, Natural Resources Canada, Ottawa, ON, Canada

Abstract

Geodetic methods are one of the few types of geophysical data that are sensitive to changes in effective pressure within operating reservoirs, albeit indirectly through induced deformation. In general, geodetic observations provide improved sampling over other existing geophysical methodologies, such as seismic time-lapse monitoring, with observation intervals varying from seconds to days, weeks or months. Satellite-based Interferometric Synthetic Aperture Radar (InSAR) are cost-effective and used in many applications including the monitoring of the injection of carbon dioxide for both long term storage and enhanced oil production. An application to the geological sequestration of carbon dioxide in Algeria revealed the northwest migration along a fault/fracture zone intersected by the injection well. A study in Texas demonstrates that enhanced oil recovery utilizing carbon dioxide leads to observable surface deformation that may be used to characterize the production and injection.

Introduction

The injection of carbon dioxide into the sub-surface, for both the long-term storage of greenhouse gases and as a method for enhanced oil production, presents a number of unique challenges. In general, due to viscosity and density effects, the behavior of the CO_2 in the subsurface can be very different from that of injected water. For example, gravitational forces can produce significant vertical movement as observed at Sleipner. The associated fluid flow may be relatively rapid and density effects can grow as fluids migrate upward. Such

complicated behavior can be problematic for efforts such as geological storage where strict accounting and long-term stability is important and in enhanced oil recovery efforts due to the costs associated with injected carbon dioxide.

Geophysical monitoring is critical in detecting deviations from the expected movement of injected CO_2. The monitoring requirements for geological storage can be quite different from those for enhanced oil recovery. The sequestration of carbon dioxide is a long-term affair and the well configuration is often fixed early, if not at the start of the effort. The injected volumes can be quite large, leading to significant changes in in-situ pore pressure and consequently the stress field in and around the injection sites. Rapid sampling in time is required at the onset of injection in order to understand the fluid flow away from the well and to identify those regions to which the carbon dioxide is migrating. During enhanced oil recovery the well geometry can be constantly changing due to evolving information and changes in production strategy. Therefore, frequent time-lapse imaging is highly desirable in order to maintain effective recovery of the oil-in-place. Seismic imaging and micro-seismic monitoring are two of the more common techniques for tracking the movement of carbon dioxide in the subsurface. However, seismic imaging can be expensive and even though sparse permanent arrays are sometimes available, they are not commonly used for frequent time-lapse imaging. Micro-seismic methods can be cost-effective but the injection of carbon dioxide may not produce ample seismicity and the events are only indirectly related to the injected fluids through the changes in stress in the subsurface.

Geodetic techniques, in which displacements are measured at the Earth's surface or in the overburden above a reservoir, are yet another geophysical tool for monitoring injected carbon dioxide. They typically have favorable temporal sampling, with observations gathered every few minutes to days or weeks apart. Geodetic observational methods are often cost-effective in comparison with seismic surveys, particularly with the availability of Interferometric Synthetic Aperture Radar (InSAR) data from orbiting satellites. Observations of surface deformation do not provide the resolution of seismic reflection imaging but they can be combined with other measurements and/or used with a detailed reservoir model to provide useful information on CO_2 movement. In this article we outline how geodetic methods may be used to monitor injection efforts and provide several examples of recent monitoring efforts.

Observational Methods

Overview

Most geodetic methods can be roughly divided into point measurement techniques, such as tilt and Global Navigation Satellite Systems (GNSS), and scanning methods, of which InSAR and Light Detection and Ranging

(LiDAR) systems are prime examples (Eitel et al. 2016). A new technique that, to some degree, bridges these two classes of observations methods, fiber optical cables for strain measurements (He et al. 2013), is currently under active development. Point observation methods typically provide much better temporal resolution, with samples gathered seconds to minutes apart, at the expense of spatial density. Scanning systems, which send an electromagnetic signal to a target and record the return, provide excellent spatial sampling but are usually gathered at time intervals of days to months apart. Local LiDAR systems, such as those used for engineering applications, can be sampled at much higher rates approaching those of point methods. A third category of observations derives from time-lapse seismic monitoring (Landro and Stammeijer 2004,). Specifically, one may extract geodetic information from the movement of reflectors in the time interval between two seismic survey (Tura et al. 2005, Staples et al. 2007, Hodgson et al 2007). In what follows we will outline two of the more commonly used techniques, InSAR and GNSS, in more detail.

Synthetic Aperture Radar Interferometry

Interferometric Synthetic aperture radar (InSAR) methods rely on the phase delay of a reflected microwave or radar wave to estimate the displacement of points on the Earth's surface (Figure 1). Both airborne and satellite-based systems are available and the methodology is now well established and widely used to map the deformation of the Earth's surface (Ferretti 2014). The accuracy of InSAR measurements depend on a variety of factors including spatial (i.e. distance between subsequent satellite passes) and temporal (i.e. time span between two acquisitions) baselines, satellite wave-length, land cover, and atmospheric conditions. To better understand the nature of InSAR observations, consider the phase of a pulse reflected from a point on the Earth, a single pixel in a SAR image (Figure 1). The phase value φ of a pixel P of a radar image can be modeled as a mixture of four distinct contributions (Ferretti 2014):

$$\varphi(P) = \vartheta + \frac{4\pi}{\lambda} r + a + n \qquad (1)$$

where ϑ is the phase shift related to the location and to the reflectivity of all elementary scatterers within the resolution cell associated with pixel P. The coefficient $4\pi r/\lambda$ is the most significant contribution in any geodetic application, as it is associated with the sensor-to-target distance or range, r. The term a is a propagation delay introduced by variations in the Earth's atmosphere. This quantity is often the main source of error and can compromise the quality of any distance estimate. The last term, n, is a phase contribution related to system noise such as thermal vibrations, quantization errors, and so on. The phase values contained in a single SAR image are of little practical use, as it is impossible to separate the different contributions in equation (1) without prior information. The basic idea of SAR interferometry is to measure the phase *change*, or interference, over time, between two radar images, generating an *interferogram* I:

$$I = \Delta\,\varphi(P) = \Delta\,\vartheta + \frac{4\pi}{\lambda}\Delta r + \Delta a + \Delta n \quad (2)$$

If we consider an idealized situation where the noise is negligible, the surface character and atmospheric conditions are constant between the two SAR acquisitions, then equation (2) reduces to

$$I = \Delta\,\varphi(P) = \frac{4\pi}{\lambda}\Delta r. \quad (3)$$

Therefore, if a point on the ground moves during the time interval between the acquisition of the two radar images with similar geometry, the distance between the sensor and the target changes, creating a phase shift proportional to the displacement (Figure 1).

The literature on InSAR techniques and applications is vast and several techniques have been developed to improve the calculation of range change. Two of the more promising approaches that have led to estimates with a precision of several milli-meters, are *permanent or persistent scatterer* techniques and *small baseline analysis*. Both methods use a sequence of inteferograms to overcome the limitations of conventional InSAR analyses, namely: phase decorrelation, i.e. possible changes in the radar signature over the area of interest, the term ϑ in equation (2), and atmospheric effects. The first method relies on the identification of point-wise, coherent, radar targets, often referred to as permanent or persistent scatterers (Ferretti et al. 2001). Permanent scatterers corresponding to radar targets with relatively constant amplitudes and slowly-varying phase that can be either natural or man-made. The Small Baseline Subset (SBAS) method (Berardino et al., 2002, Lanari et al. 2004, Hooper 2008, Samsonov et al., 2011, Samsonov and d'Oreye 2012) selects many coherent interferograms acquired with small spatial and temporal baselines, solves for the deformation rates between subsequent SAR acquisitions and then reconstructs time series of the cumulative displacements. Various deformation time series analysis software packages are available, including StaMPS (Hooper et al., 2016), GIAnT (Agram et al., 2013), and Parallel-SBAS (Casu et al., 2014).

Global Navigation Satellite Systems

Originally developed by the US Department of Defense, this approach relies on the triangulation of signals from orbiting satellites to estimate three-dimensional positions and displacements to the precision of a few millimeters (Figure 2). Other nations have deployed similar satellite navigation systems, and the combined suite of systems are known as GNSS (Global Navigation Satellite Systems). Several aspects of GNSS geodesy are similar to the InSAR technique. Both techniques use coherent microwave signals, make phase measurements on these signals, and suffer from noise associated with signal propagation through the atmosphere. Both techniques also require high precision satellite orbits to be computed and available for the data analysis. Unlike

InSAR, GNSS is an absolute positioning technique, using measurements of range to four or more satellites to uniquely define a point position on the Earth's surface. Another difference between InSAR and GPS is that fine time resolution is possible with global satellite systems. The high precision of GNSS position and displacement measurements reflects several characteristics of the system. For example, most of these systems use dual frequency measurements, allowing a first order correction for ionospheric effects. Second, the ability to make large numbers of range and phase change measurements to a number of satellites simultaneously, over different viewing angles, allows a first order correction for the atmospheric delay due to water vapor. Other effects that influence the position of a point on the Earth's surface at the millimeter to centimeter level, such as Earth tides, ocean loading, and changes in Earth orientation are corrected during data analysis via models or measurements from other space geodetic techniques. The availability of GNSS has opened up a host of geological and geophysical applications, such as measurement of ground deformation associated with extraction or injection of fluids, including injection of CO_2. There are a number of technical books on the subject for readers interested in more detail, including Teunissen and Kleusberg (1998) and Hofmann-Wellenhof et al. (2007). Geophysical applications are reviewed in Dixon (1991), Bürgmann and Thatcher (2013) and Bock and Melgar (2016).

Data Interpretation and Inversion Methods

Changes in the fluid volume within a reservoir leads to variations in the effective pressure, that is the difference between the total pressure and the fluid pressure, inducing deformation and stress changes within the reservoir and the surrounding rock. Under favorable conditions the resulting stress and strain lead to observable surface deformation. To make use of these observations we need to relate the surface deformation to reservoir processes. There are several levels of sophistication can be used to describe this relationship. At the simplest level, we can relate the surface deformation directly to reservoir volume change without considering the fluid pressure changes that led to the volume change. Thus, we restrict ourselves to purely mechanical considerations and are not concerned with modeling the fluid flow leading to the volume change. This approach involves the fewest model parameters, and if we are interested in short time intervals, can usually be accomplished using an elastic or poroelastic model for the overburden (Vasco et al. 2010). More sophisticated simulations of the fluid flow within the reservoir can also improve the fidelity of the modeling, at the expense of introducing additional, often unknown, parameters such as reservoir permeability and porosity. The most advanced level involves modeling both the fluid flow and the deformation using a coupled numerical simulator

The simplest conceptual model used to relate the deformation to volume changes in the reservoir is similar to that applied in seismic source estimation and imaging. That is, though the source volume may undergo non-linear deformation and strain, outside of the source region the much smaller deformation of the surrounding rock can be described using methods from linear elasticity over the time interval between surveys, typically less than one month. In particular, one can use a Green's function, $G_i(\mathbf{x}, \boldsymbol{y})$, or impulse response function to relate the displacements of the overburden $u_i(\mathbf{x})$ to the fractional volume change, $\Delta v(\boldsymbol{y})$, within the reservoir

$$u_i(\boldsymbol{x}) = \int_V G_i(\mathbf{x}, \boldsymbol{y}) \Delta v(\boldsymbol{y}) d\boldsymbol{y} \qquad (1)$$

where V is the reservoir volume (Rucci et al. 2013). The Green's function depends upon the elastic properties of the overburden and the effort required for its computation depends upon the complexity of this elastic model. There are analytic and semi-analytic techniques for homogeneous half-space and layered models, respectively, and numerical finite-difference and finite-element methods may be applied to fully three-dimensional models. The forward problem entails computing the displacements in the overburden given a distribution of volume change within the reservoir.

The inverse problem consists of using observations of the deformation of the overburden to estimate volume change within the reservoir. This is a much more difficult task because of the loss of resolution with depth, due to the smoothing effects of the Green's function in equation (1). However, an inversion of the deformation can be formulated as a least squares minimization problem and one can take advantage of the linearity of equation (1) in solving for the spatial distribution of the reservoir volume change (Rucci et al. 2013). Due to the difficulty of the inverse problem it is important to devise appropriate regularization schemes to stabilize the process of estimating a solution. One particularly useful approach for volume changes that are induced by fluid extraction and injection into a reservoir, is a regularization or penalty term that favors volume changes near known well locations (Vasco et al. 2010, Rucci et al. 2013, Vasco et al. 2019). Such a penalty term utilizes the fact that the effective pressure changes surrounding the well are driving the volume changes within the reservoir. Conventional regularization terms, such as model norm and roughness penalty functions tend to produce excessively smooth solutions, exacerbating the loss of resolution with depth. Another way to regularize the inverse problem is via a model parameterization that accounts for known aspects of the source. For example, if the fluid volume changes are restricted to a specific formation with known boundaries one can incorporate that fact by restricting the source volume to that region. Similarly, if the deformation is thought to be due to an evolving fracture/fault zone, then the source change be modeled as aperture changes distributed over the potential fracture/fault plane

Applications

Carbon Sequestration at In Salah, Algeria

The In Salah gas storage project sequestered excess carbon dioxide that was stripped from natural gas produced from three fields in Algeria. The reservoir itself is a thin, roughly 20 m thick, layer that forms a gentle anticline overlain by approximately 2 km of shale and sandstone (Figure 3). Beginning in 2004 the first of three horizontal wells began injecting the separated carbon dioxide into the formation. Fortunately, observations from a SAR satellites of the European Space Agency were available, as the satellite had been gathering data for several years prior to the start of injection. An early analysis revealed significant range change due to uplift over each of the three injectors (Figure 4). Interestingly, a double-lobbed pattern, indicative of the opening of a narrow vertical feature such as a fault or fracture, was observed over the injection well KB-502. This conclusion was supported at wells KB-502 and KB-503 by a later seismic survey that detected push-down in a narrow fault/fracture zones due to the injected carbon dioxide (Gibson-Poole and Raikes 2010), as shown in Figure 5.

Based upon the suggestion of fault/fracture flow, the source of the uplift above well KB-502 was modeled as a vertical damage zone that responds to the injection of the carbon dioxide by increases in aperture or fracture width. The trace of the fracture zone is plotted on top of the seismic push-down in Figure 5. Using the modeling technique presented in equation (1) it is possible to formulate an inverse problem for the aperture changes of discrete patches of the fault/fracture zone as a function of time, indicative of the movement of the carbon dioxide through the subsurface. That is, we can relate the InSAR range change, $r(\mathbf{x}_j, t)$, at a location $\mathbf{x}_j$ on the Earth's surface to the aperture changes on rectangular patches over the vertical fracture

$$r(\mathbf{x}_j, t) = \sum_{n=1}^{N} R_n(\mathbf{x}_j) a_n(t) = \mathbf{R}(\mathbf{x}_j) \cdot \mathbf{a}(t)$$

where $R_n(x_j)$ is the integral of the projection of the Green's functions of the three displacement components along the look vector, $\mathbf{l}$, taken over the fault/fracture patch P_n:

$$R_n(\mathbf{x}_j) = \int_{P_n} l_i \cdot G_i(\mathbf{x}_j, y) dV$$

Given a set of range change measurements, roughly 300,000 total observations at the In Salah site (Figure 4), we can write the associated collection of linear constraints as a large system of equations for the aperture changes over the fault/fracture surface. The inverse problem entails solving this linear system for the aperture changes during each time interval. This is accomplished using a least squares approach where we minimize the

sum of the squares of the residuals. In order to stabilize the inverse problem, we introduce a term which penalizes aperture changes that are far from the known well location. This penalty function is based upon the hypothesis that the aperture changes are driven by fluid pressure changes due to injection and that these changes are largest near the well itself. Therefore, we minimize the composite quadratic function in the aperture $\mathbf{a}(t)$,

$$Q(\mathbf{a}) = (\mathbf{d} - \mathbf{M}\mathbf{a})^t \cdot (\mathbf{d} - \mathbf{M}\mathbf{a}) + \mathbf{a}^t \mathbf{D}\mathbf{a}$$

where $\mathbf{d}$ is the matrix of observed range changes, the data, $\mathbf{M}$ is a matrix with the j-th row given by $\mathbf{R}(\mathbf{x}_j)$, and a diagonal penalty matrix $\mathbf{D}$, that takes on large values for cells that are far from the injection well. The necessary equations for the minimum of the quadratic function $Q(\mathbf{a})$, with respect to the components of the aperture vector $\mathbf{a}$, produces the desired linear system of equations.

Aperture changes for a selected set of time intervals, obtained by inverting the InSAR range changes above injection well KB-502, are shown in Figure 6. Note the northwestward migration of the CO_2 for several kilometers from the injection well during the first two years of sequestration. Such rapid migration was validated by the relatively rapid appearance of carbon dioxide at an unused well to the northwest (Mathieson et al. 2010, Ringrose et al. 2013), and by the subsequent seismic survey (Gibson-Poole and Raikes 2010), as indicated by the narrow corridor of push-down extending several kilometers to the northwest of the injection well (Figure 5). The stress changes associated with the migrating carbon dioxide have generated micro-earthquakes that were detected by an array of seismometers that was installed in 2009, well after the start of injection in KB-502. The vast majority of microseismic events are located at or below the injection well, supporting the conclusion that the CO_2 remained at depth (Stork et al. 2015), as in the solution plotted in Figure 5. The restriction on the depth of the injected carbon dioxide to within a few hundred meters of the injection well is also supported by coupled geomechanical modeling (Rinaldi and Rutqvist 2013) and a stochastic inversion of the InSAR data (Ramirez and Foxall 2014).

Monitoring Enhanced Oil Recovery at the Kelley-Snyder field, Texas

In addition to storage and long-term sequestration, carbon dioxide may be injected to maintain or increase reservoir pressure and reduce viscosity, a technique for enhanced oil recovery (EOR). Monitoring of surface deformation in a field undergoing EOR provides a check on reservoir pressure changes and fluid pathways. Data analysis and modeling are similar to the procedures described above for carbon sequestration, with one significant difference: in actively producing fields, fluids are both injected and extracted concurrently. In addition, there are often large numbers of injection and production wells. Hence, it is important to account for

the various cumulative fluid fluxes and their relative contributions to reservoir pressure, which can involve complex book-keeping and equation of state calculations.

Here we describe an example from the west Texas Kelley-Snyder oil field (Figure 7), that is presented in more detail in Yang et al. (2015). The reservoir, with an average depth of 2,000 meters, consists of sub-surface limestone reef mounds, including the Pennsylvanian age Cisco and Canyon formations (Yang et al. 2015). The field has been an important producer since the early 1950's. Production declines on the 1960's led to injection of water, followed by injection of CO_2 in the early 1970's. Injection of carbon dioxide increased significantly in the early 2000's and a total of 100 Mega-tonnes was injected into the field between 1972 and 2011. Data from the Japanese Aerospace Exploration Agency ALOS-1 SAR satellite, with a repeat time of 46 days, were gathered over the field. The data set consists of 13 SAR images collected between 2007 and 2011. These data where used to generate 53 interferograms. The Small Baseline Subset technique was used to generate a range change time series that measured up to 10 cm of uplift, closely centered on the reservoir (Figure 7).

The field operator provided injection and production data for the hundreds of wells operating in the field. The injected and produced volumes were summed in 500 m by 500 m grid blocks (Figure 8). A matched asymptotic solution for reservoir pressure (Mathias et al. 2009), accounting for two phase flow (supercritical carbon dioxide and water), was coupled with an analytic expression for surface deformation (Xu et al. 2012) in order to understand the flow and the pressure distribution within the reservoir, and to establish the compatibility between the production-injection and the observed range change (Yang et al. 2015). Thus, the approach uses a simplified method to compute the Green's function for the forward modeling discussed above. The contribution from each effective block was summed to estimate the total fluid pressure changes cause by the injection and production (Figure 9). Computation of the range change at the surface, due to the pressure distribution in Figure 9, required an estimate of the Young's modulus of the half-space model. Estimates were obtained by conducting a series of inversions with varying values of Young's modulus and finding the value that minimized the misfit (Figure 10). Given an optimal Young's modulus the pressure variations in Figure 9 were used to estimate the range change at the surface, using the method of Xu et al. (2012). The calculated range change match the InSAR observations (Figure 11) with some exceptions to the south of the field, where there is a systematic residual of around 4 cm. The discrepancy may be due to atmosphere effects or the effects of shallow aquifers in the region. The range change data at the Kelley-Synder field may also be used to invert for fluid pressure changes and to estimate spatial variations in reservoir permeability, as in Vasco et al. (2008).

Discussion: Limitations and Advancements

Our examples provide two cases in which surface deformation is sufficient to provide constraints on fluid flow at depth. Another example related to CO_2 EOR is provided by the GNSS-based study of Karegar et al. (2015). While there are a large number of situations where this is feasible, there are also significant areas where injection and production do not generate significant surface deformation. The conditions for generating observable deformation are not yet understood and the generation of stress changes in the subsurface due to injection and production can be complicated, as can be the relationship between seismicity and ground deformation (Shirzaei et al. 2016). Improved understanding should come with better modeling and accounting for the variations in poroelastic properties within the Earth. Furthermore, advancements in instrumentation and monitoring techniques should lead to improved detection, particularly for methods that provide observations at depth and do not rely on surface measurements. One class of methods are the time-lapse seismic time strains mentioned earlier (Hatchell and Bourne 2005, Tura et al. 2005, Staples et al. 2007). These methods provide observations at locations where the strain is much larger than at the Earth's surface and have the potential to greatly enhance our resolution of pressure changes (Hodgson et al. 2007), as indicated in Figure 12. Another class of downhole observations, that is just now undergoing active development, is provided by fiber-optic cables and distributed strain sensing (He et al. 2013). This technology can provide observations where there are wells, extending measurements right into the areas of interest. It should be possible to combine such geodetic data with microseismicity to better understand processes such as fracture development.

Conclusions

Both the geological sequestration of carbon dioxide and enhanced oil production utilizing CO_2 result in changes in effective pressure that lead to observable surface deformation. These observations provide information on subsurface fluid flow, as demonstrated here, can provide the foundation for an inverse problem for reservoir volume change or aperture change on an evolving fracture. One can formulate these inverse problems in purely mechanical terms, without the need for reservoir simulation or coupled fluid flow and geomechanics. This reduces the number of unknown parameters to reservoir volume changes or aperture changes. The temporal resolution of geodetic data allow for rapid results and quick turn-around times for imaging.

References

Agram, P. S., R. Jolivet, B. Riel, Y. N. Lin, M. Simons, E. Hetland, M. P. Doin and C. Lassere, 2013, New Radar Interferometric Time Series Analysis Toolbox Released, Eos Trans. AGU, 94, 69

Berardino, P., Fornaro, G., Lanari, R., 2002. A new algorithm for surface deformation monitoring based on small baseline differential SAR interfereograms. IEEE transactions on Geoscience and Remote Sensing 40 (11), 2375-2383.

Bock, Y. and Melgar, D. (2016) Physical applications of GPS geodesy: a review. *Reports on Progress in Physics*, 79, 10, 106801.

Bürgmann, R., Thatcher, W. (2013) Space geodesy: A revolution in crustal deformation measurements of tectonic processes. *Geological Society of America, Special Paper* 500.

Casu, F., S. Elefante, P. Imperatore, I. Zinno, M. Manunta, C. De Luca, R. Lanari , "SBAS-DInSAR Parallel Processing for Deformation Time-Series Computation," in *IEEE Journal of Selected Topics in Applied Earth Observations and Remote Sensing*, vol. 7, no. 8, pp. 3285-3296, Aug. 2014. doi: 10.1109/JSTARS.2014.2322671

Dixon, T. H. (1991) An introduction to the Global Positioning System and some geological applications, *Reviews of Geophysics*, **29**, 249-276.

Eitel, J. U. H., Hofle, B., Vierling, L. A., Abellan, A., Asner, G. P., Deems, J. S., Glennie, C. L., Joerg, P. C., Lewinter, A. L., Magney, T. S., Mandlburger G., Morton, D. C., Muller, J., and Vierling, K. T. (2016). Beyond 3-D: The new spectrum of lidar applications for earth and ecological sciences, *Remote Sensing of Environment*, **186**, 372-392.

Ferretti, A., Prati, C. and Rocca, F. (2001). Permanent Scatterers in SAR Interferometry, *IEEE Transactions on Geoscience and Remote Sensing*, **39**(1), 8 -20.

Ferretti, A. (2014). *Satellite InSAR Data – Reservoir Monitoring from Space*. EAGE Publications.

Gibson-Poole, C. M., and Raikes, S., (2010). Enhanced understanding of CO_2 storage at Krechba from 3D seismic, in *Proceedings of the 9th Annual Conference on Carbon Capture and Sequestration*, Pittsburgh, PA, May 10-13.

He, Z. Liu, Q., and Tokunaga, T. (2013). Unitrahigh resolution fiber-optic quasi-static strain sensors for geophysical research, *Photonic Sensors*, **3**, 295-303.

Hodgson, N., MacBeth, C., Duranti, L., Rickett, J. and Nihei, K. (2007). Inverting for reservoir pressure changes using time-lapse time strain: Application to the Genesis Field, Gulf of Mexico, The Leading Edge, May, 649-652.

Hofmann-Wellenhof, B., Lichtenegger, H. and Wasle, E. (2007) *GNSS-Global Navigation Satellite Systems: GPS, GLONASS, Galileo, and More* (Wien: Springer).

Hooper, A. (2008). A multi-temporal InSAR method incorporating both persistent scatterer and small baseline approaches, *Geophysical Research Letters***, 35**, L16302, 1-5.

Hooper, A., D. Bekaert, K. Spaans, M. Arikan, 2012, Recent advances in SAR interferometry time series analysis for measuring crustal deformation, Tectonophysics, 514-517, pp.1-13, doi:10.1016/j.tecto.2011.10.013

Karegar, M. A., T. H. Dixon, Q. Yang, R. Malservisi, S. A. Hossaini, *S.* D. Hovorka (2015) GPS-based Monitoring of Surface Deformation Associated with CO_2 Injection at an Enhanced Oil Recovery Site, *International Journal of Greenhouse Gas Control* 41, 116-126, doi: 10.1016/j.ijggc.2015.07.006

Lanari, R., Mora, O., Manunta, M., Mallorqui, J. J., Berardino, P, and Sansosti, E. (2004). A small baseline approach for investigating deformations on full-resolution differential SAR interferograms, *IEEE Transactions on Geoscience and Remote Sensing*, **42**, 1377-1386.

Mathias, S. A., Hardisty, P. E., Trudell, M. R., and Zimmerman, R. W. (2009). Approximate solutions for pressure buildup during CO2 injection in brine aquifers, *Transport in Porous Media*, **79**, 265-284.

Mathieson, A. Midgley, J., Dodds, K., Wright, I., Ringrose, P., and Saoula, N. (2010). CO2 sequestration monitoring and verification technologies applied at Krechba, Algeria, *The Leading Edge*, **29**, 216-222.

Ramirez, A., Foxall, W. (2014). Stochastic inversion of InSAR data to assess the probability of pressure penetration into the lower caprock at In Salah, *International Journal of Greenhouse Gas Control,* **27**, 42-58.

Rinaldi, A. P., and Rutqvist, J. (2013). Modeling of deep fracture zone opening and transient ground surface uplift at KB-502 CO_2 injection well, In Salah, Algeria, *International Journal of Greenhouse Gas Control*, **12**, 155-167.

Ringrose, P. S., Mathieson, A. S., Wright, I. W., Selama, F., Hansen, O., Bissell, R., and Midgley, J. (2013). The In Salah CO2 storage project: lessons learned and knowledge transfer, *Energy Procedia*, **37**, 6226-6236.

Rucci, A., Vasco, D. W. and Novali, F. (2013). Monitoring the geologic storage of carbon dioxide using multicomponent SAR interferometry. *Geophysical Journal International*, **193**(1), 197-208.

Samsonov, S., d'Oreye, N. (2012). Multidimensional time series analysis of ground deformation from multiple InSAR data sets applied to Virunga Volcanic Province. Geophys. J. Int. 191, 1095-1108, http://dx.doi.org/10.1111/j.1365-246X.2012.05669.x.

Samsonov S., van der Koij M. and Tiampo, K., 2011. A simultaneous inversion for deformation rates and topographic errors of DInSAR data utilizing linear least square inversion technique, Computers & Geosciences, 37 (8), 1083-1091

Shirazaei, M., Ellsworth, W. L., Tiampo, K. F., Gonzalez, P. J., and Manga, M. (2016). Surface uplift and time-dependent seismic hazard due to fluid injection in eastern Texas, *Science*, **353**, 1416-1419.

Staples, R. Ita, J., Burrell, Rhian, and Hash, R. (2007). Monitoring pressure depletion and improving geomechanical models of the Shearwater Field using 4D seismic, *The Leading Edge*, May, 636-642.

Stork, A. L., Verdon, J. P., and Kendall, J.-M. (2015). The microseismic response at the In Salah Carbon Capture and Storage (CCS) site, *International Journal of Greenhouse Gas Control*, **32**, 159-171.

Teunissen P J, Kleusberg A. (1998) *GPS for Geodesy* (Berlin: Springer)

Tura, A., Barker, T., Cattermole, P., Collins, C., Davis, J., Hatchell, P., Koster, K. Schutjens, P., and Wills, P. (2005). Monitoring primary depletion reservoirs using amplitudes and time shifts from high-repeat seismic surveys, *The Leading Edge*, December, 1214-1221.

Vasco, D. W., Ferretti, A., and Novali, F. (2008). Estimating permeability from quasi-static deformation: Temporal variations and arrival time inversion, *Geophysics*, **73**, O37-O52.

Vasco, D. W., Rucci, A., Ferretti, A., Novali, F., Bissell, R. C., Ringrose, P. S., Mathieson, A. S., and Wright, I. W., (2010), Satellite-based measurements of surface deformation reveal fluid flow associated with the geological storage of carbon dioxide, *Geophysical Research Letters*, **37**, L03303, 1-5, doi:10.1029/2009GL041544.

Vasco, D. W., Farr, T. G., Jeanne, P., Doughty, C., and Nico, P. (2019). Satellite-based monitoring of groundwater depletion in California's Central Valley, *Nature Scientific Reports*, **9**, 16043, doi.org/10.1038/s41598-019-52371-7.

Xu, Z., Fang, Y., Scheibe, T. D., and Bonneville, A. (2012). A fluid pressure and deformation analysis for geological sequestration of carbon dioxide, *Computers in Geoscience*, **46**, 31-37.

Yang, Q., W. Zhao, T. H. Dixon, F. Amelung, W. S. Han, P. Li (2015) InSAR monitoring of ground deformation due to CO_2 injection at an Enhanced Oil Recovery Site, West Texas. *International Journal of Greenhouse Gas Control* **41**, 116-126, doi:10.1016/j.ijggc.2015.06.016

ACKNOWLEDGEMENTS

This work at Lawrence Berkeley National Laboratory was supported by the GEOSEQ project for the Assistant Secretary for Fossil Energy, Office of Coal and Power Systems, through the National Energy Technology Laboratory of the U. S. Department of Energy under contract DE-AC02-05-CH11231.

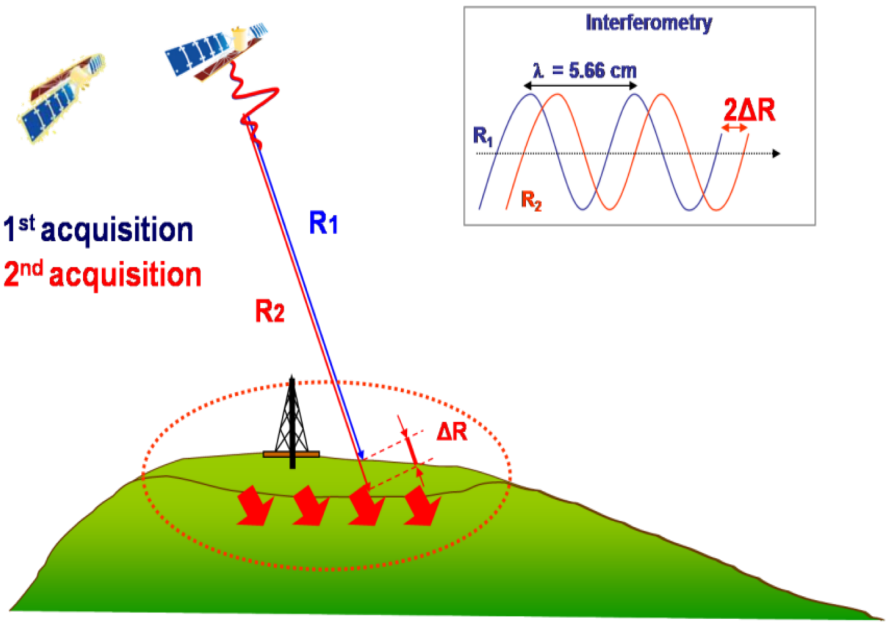

Figure 1. Illustration of the estimation of displacement along the line-of-sight to the satellite, known as the range, from the phase shift between the reflected electromagnetic waves. R1 and R2 denote the ranges from two different satellite passes, acquisition 1 and 2. The insert shows the phase shift or waveform delay of the repeat pass R2 with respect to the initial pass R1. λ is the wavelength of the radar/microwave chirp sent from the satellite, 5.66 cm in this case.

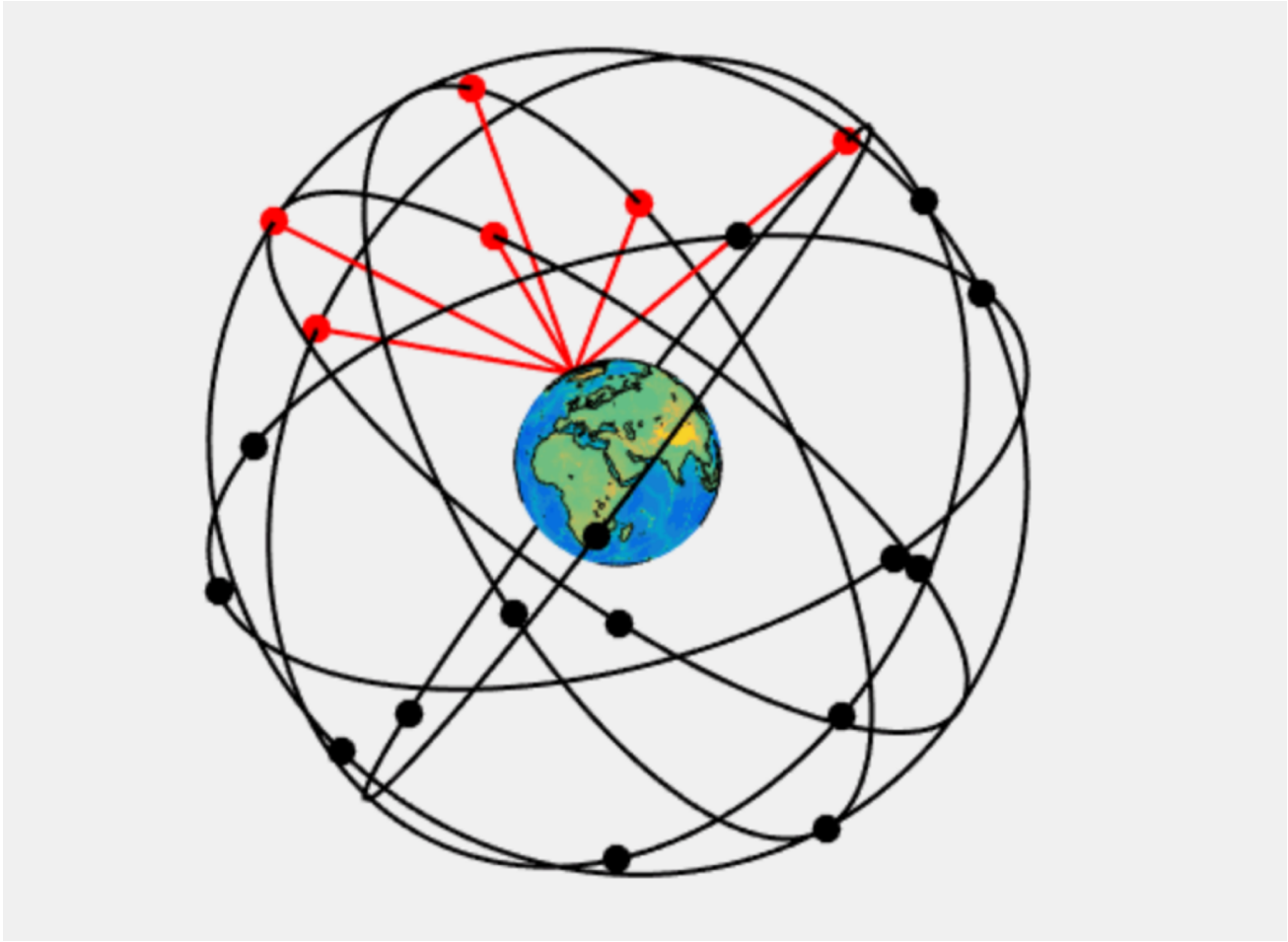

Figure 2. Schematic map of a GNSS, where the orbiting satellites are denoted by dots and their orbits by black paths. The red dots signify the satellites that are visible to a point of interest at the Earth's surface, the red lines represent the transmission paths from the satellites to that point.

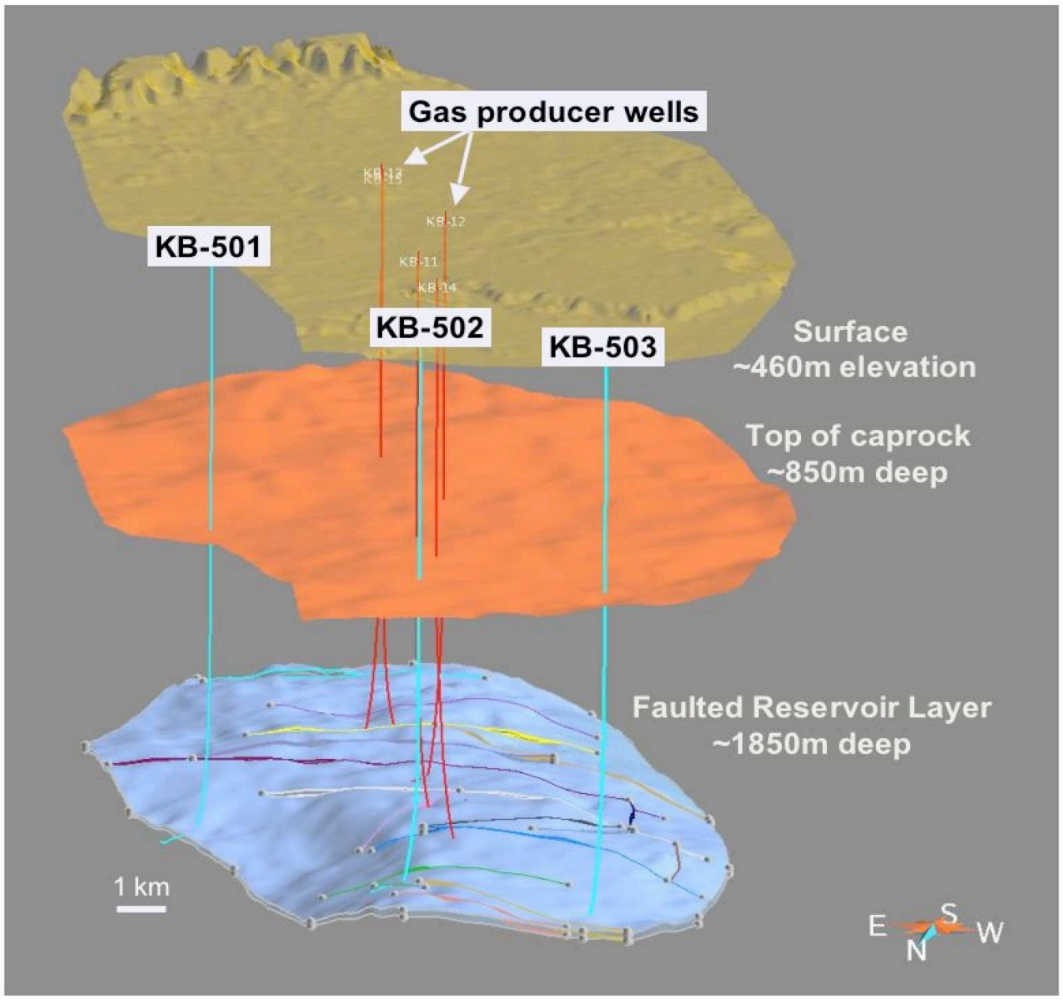

Figure 3. General structural setting and well placement at the In Salah gas storage site in Algeria.

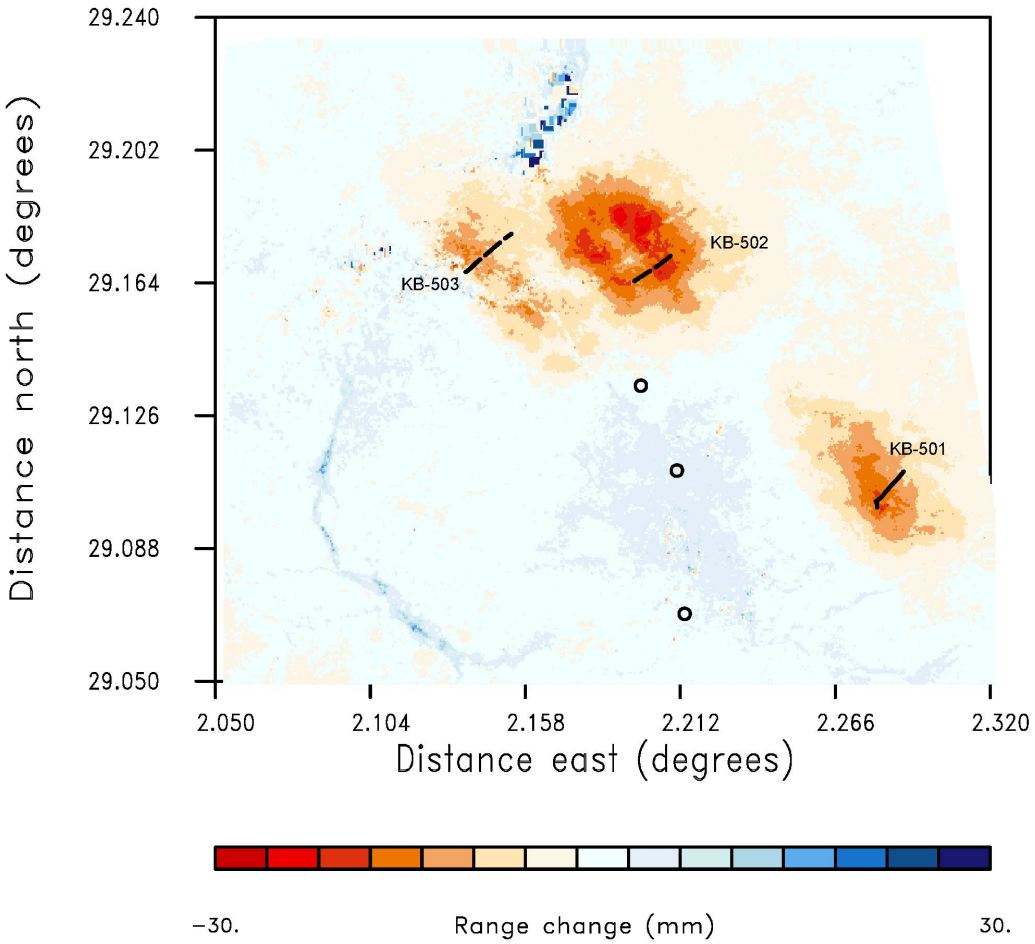

Figure 4. Range change associated with the injection of carbon dioxide at the In Salah gas storage project in Algeria. The horizontal sections of the injection wells that lie in the reservoir are indicated by the solid lines and the wells are labelled. The open circles indicate the well heads of the gas production wells from the main field.

.

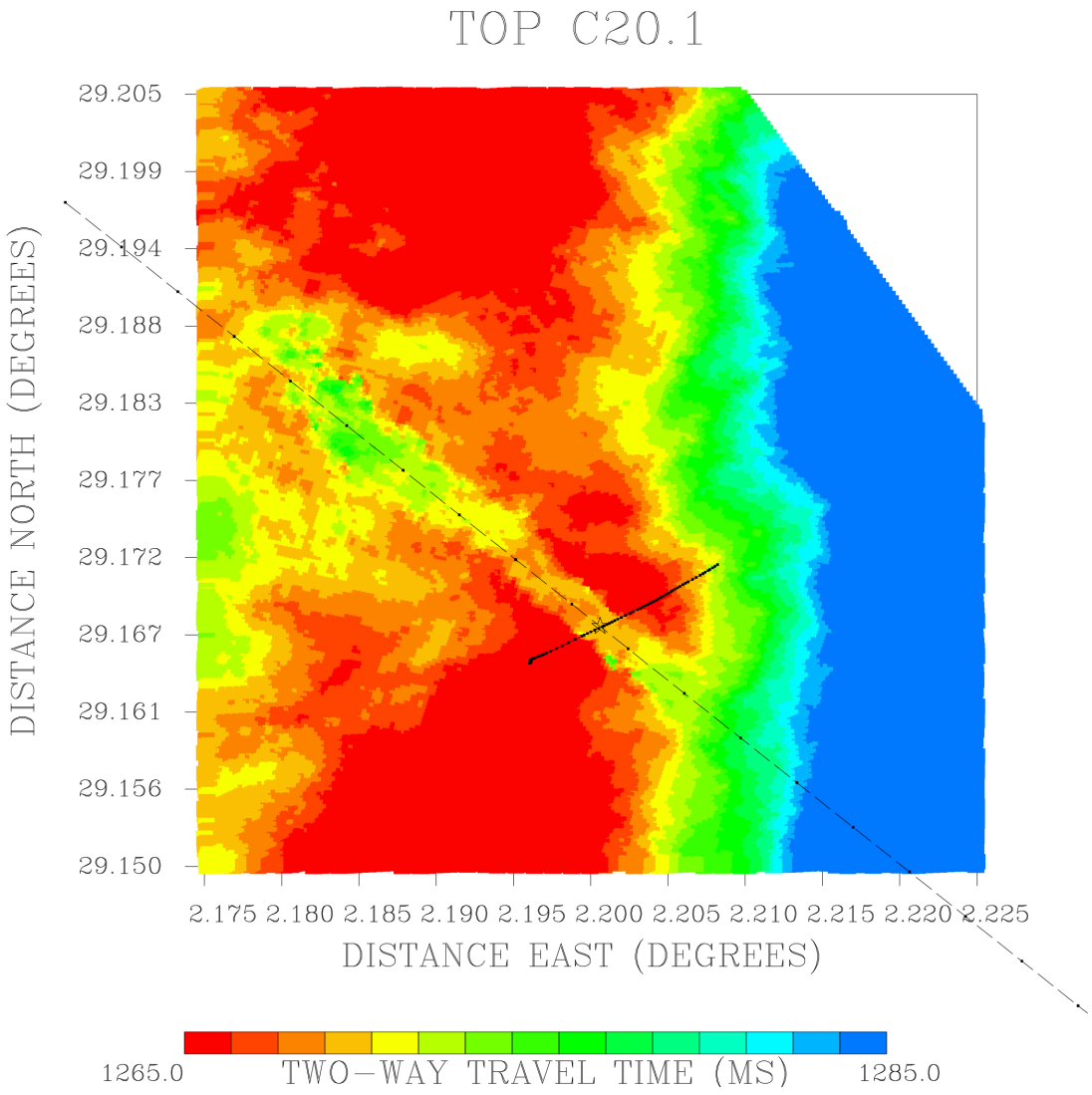

Figure 5. Compressional wave two-way travel time to the base of the storage interval. The push-down in time due to the injection of carbon dioxide is visible as a northwest trending linear feature. The axis of the travel time anomaly, indicated by the dashed line, was used to define the fault/fracture zone used in the inversion. The solid black line denotes the track of the horizontal well KB-502 within the storage formation.

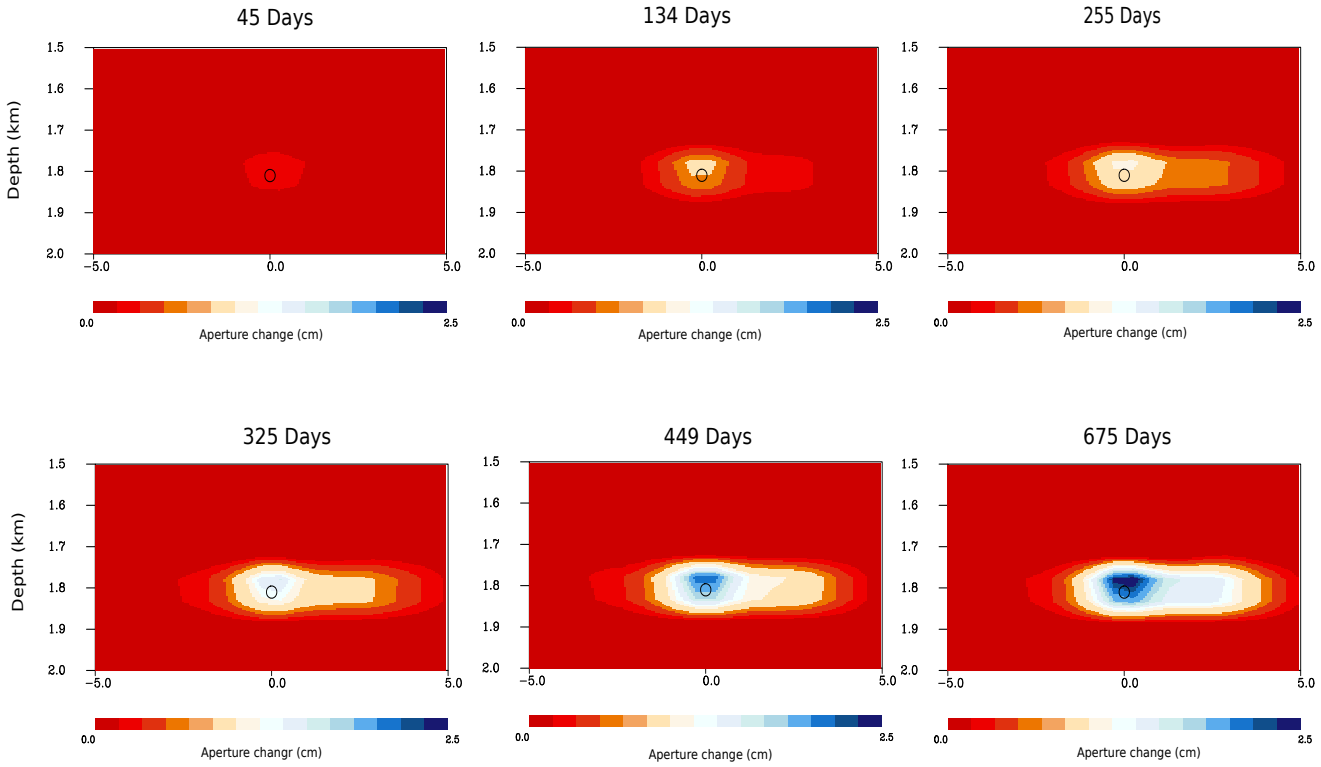

Figure 6. Aperture change during the six intervals since the start of injection at well KB-502. The horizontal axis signifies the distance to the northwest of the injection well, along the fracture trace indicated in Figure 5.

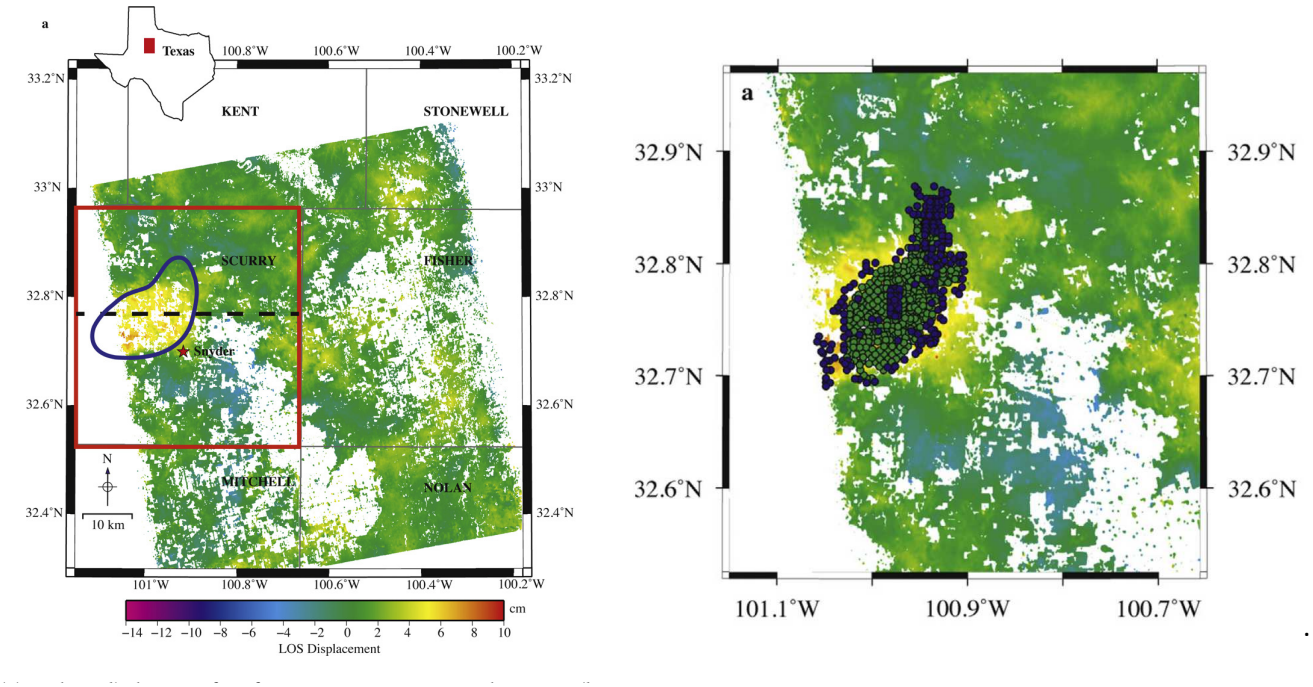

Figure 7. (Left panel) Location map showing the position of the Kelley-Snyder field in Texas. The color variations indicate the line-of-sight displacements from January 8, 2007 through March 6, 2011. (Right panel). Injection wells for carbon dioxide (green circles) and water (blue circles) plotted on top of a map of the InSAR range changes over the field..

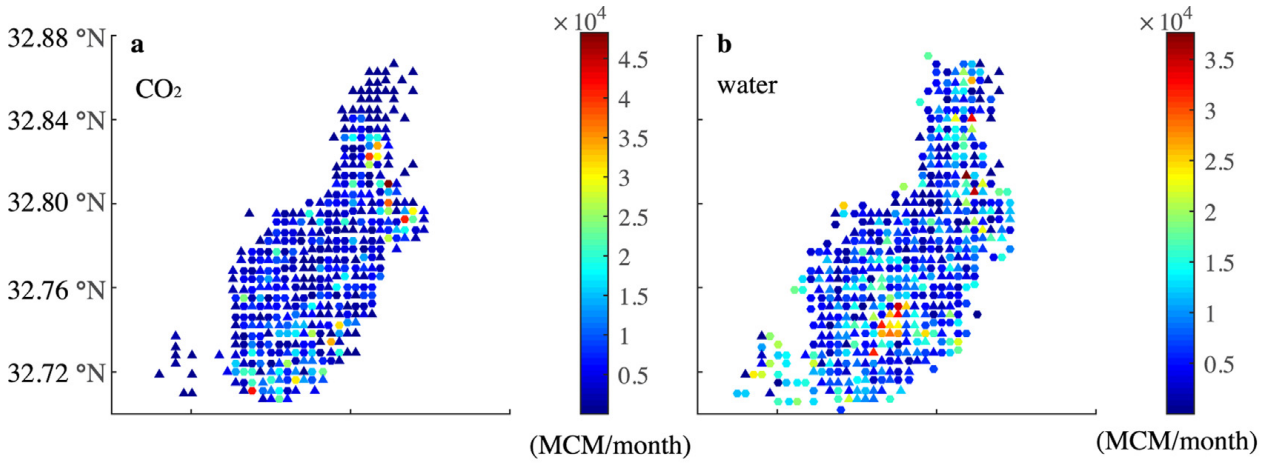

Figure 8. Location of net injection points representing effective injected volumes of (a) carbon dioxide and (b) water. Circles represent injection wells and triangles represent production wells. The injected and produced volumes correspond to conditions at 16 MPa and 41.5 C.

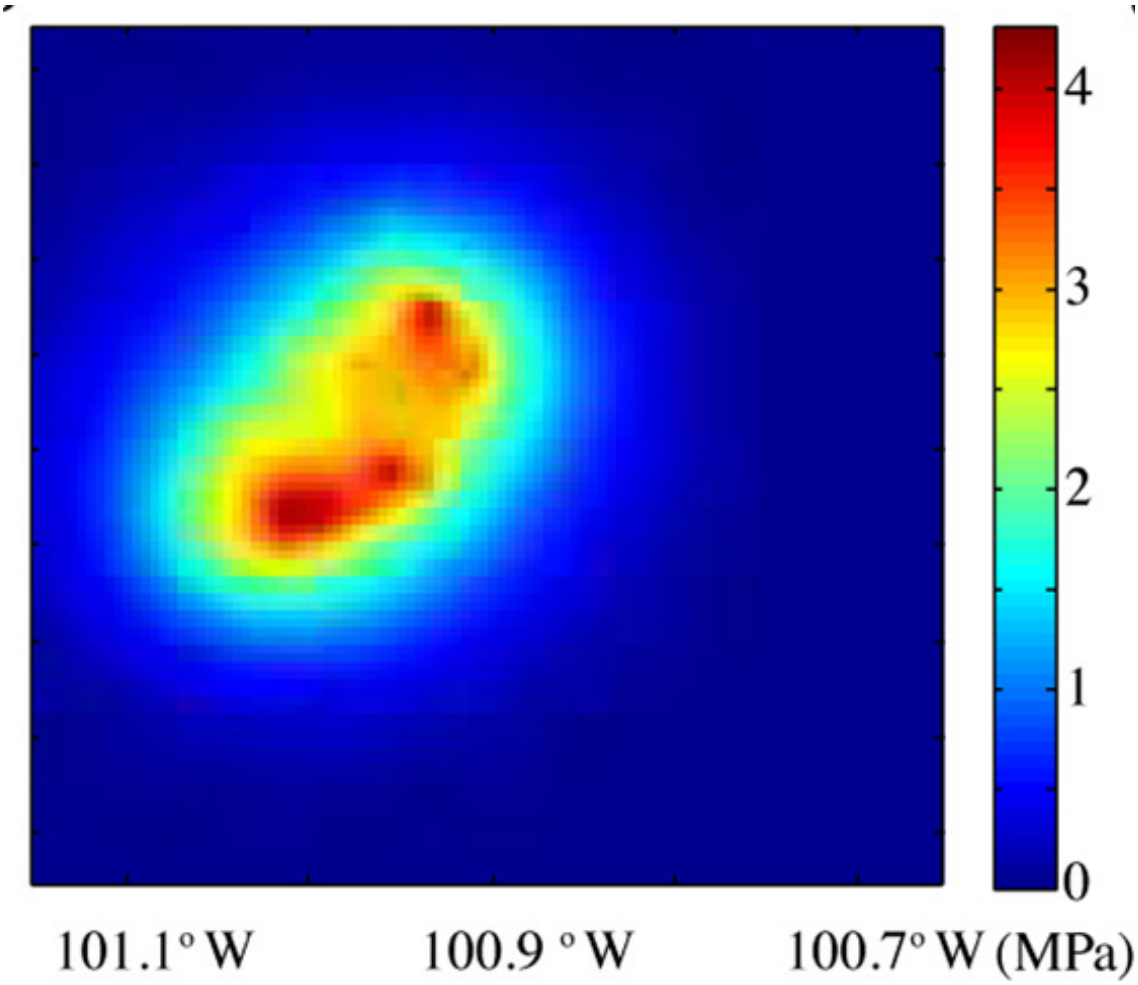

Figure 9. Calculated pressure changes due to the net fluid injection in the Kelley-Snyder field.

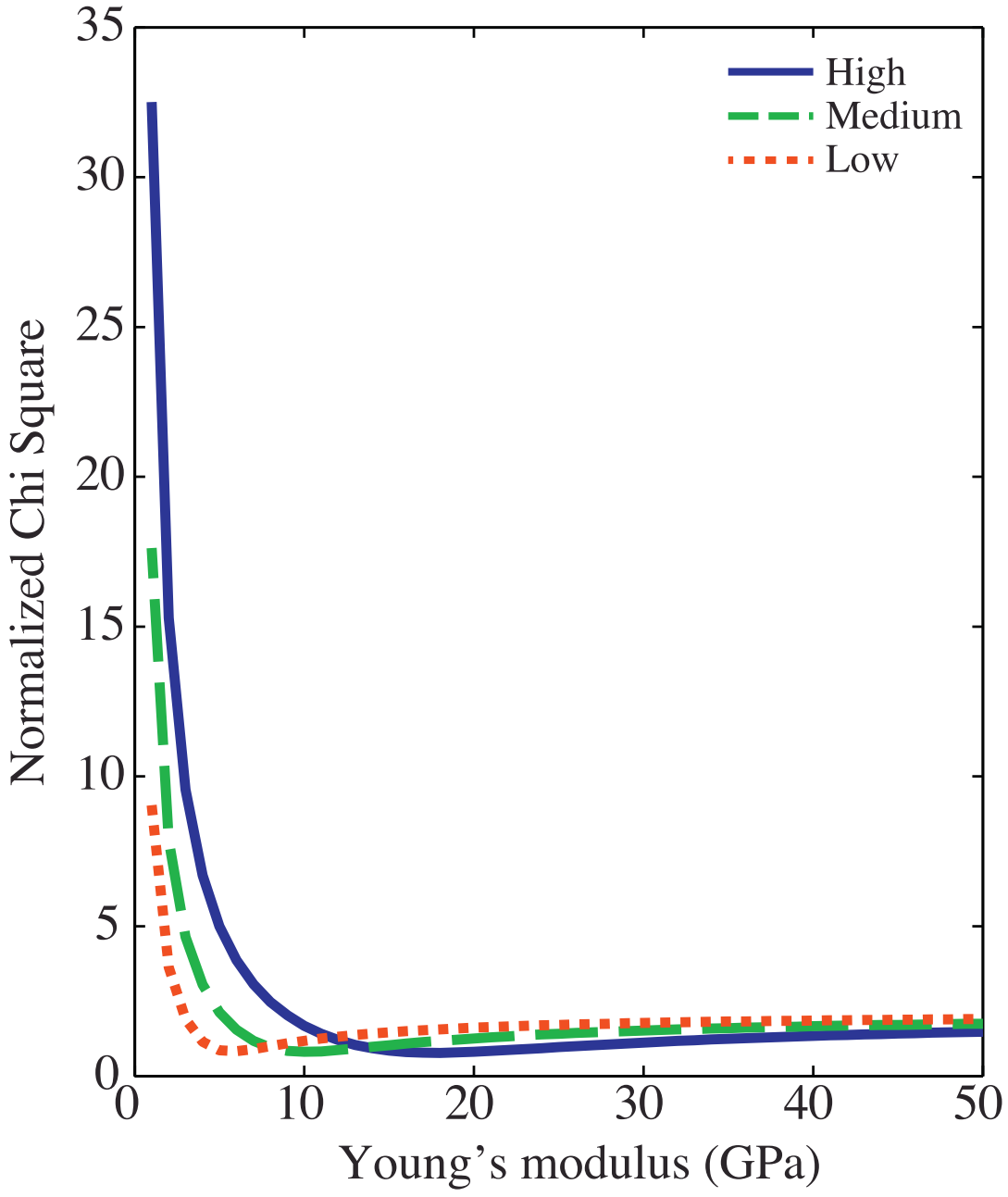

Figure 10. Misfit versus the values of Young's modulus at three levels of pressure change conditions.

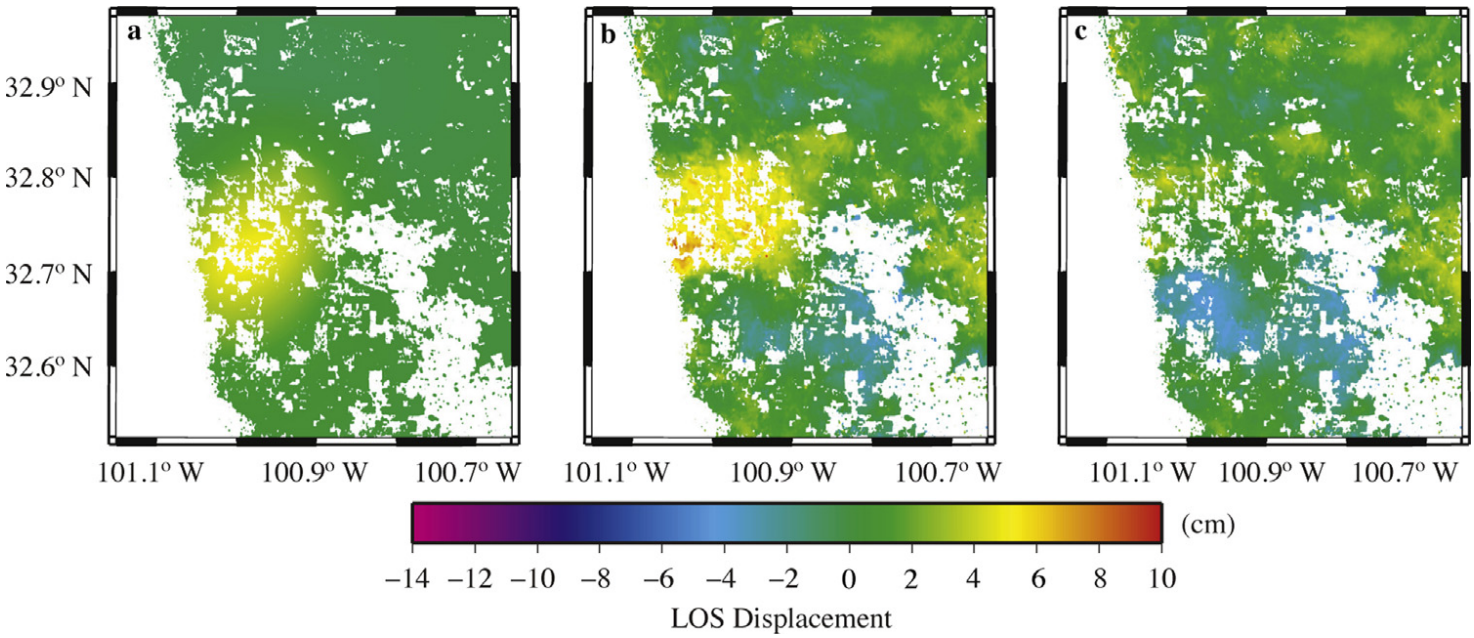

Figure 11. Comparison between (a) calculated line-of-sight displacements, (b) InSAR observations, and (c) data residuals.

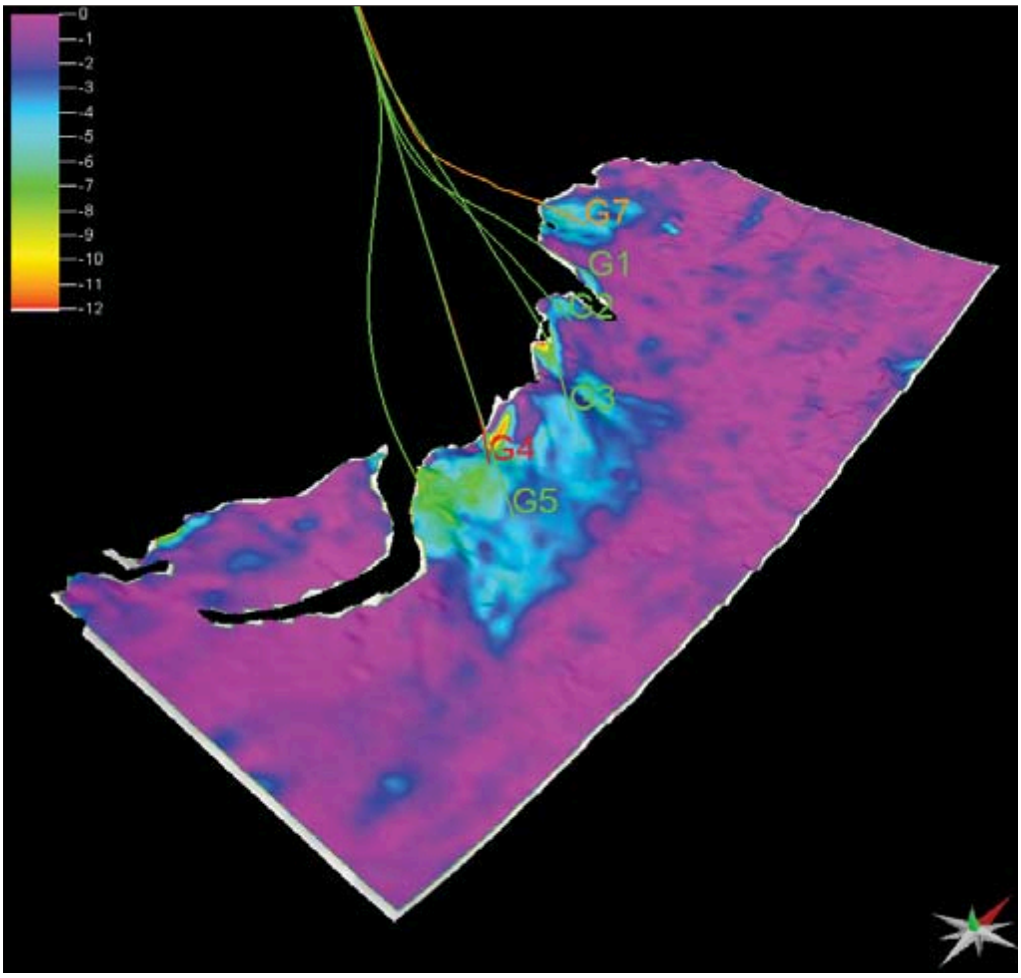

Figure 11. Seismic time shifts, from 0 to -12 ms, at the top of the first producing interval of the Genesis field. Most of the time shift can be attributed to a velocity reduction in the overburden due to a dilation of the overburden.